Hydrogen Assisted Ductile Fracture of Spheroidized Carbon Steels

R. GARBER, I. M. BERNSTEIN, AND A. W. THOMPSON

The effects of hydrogen on ductile fracture were studied in two spheroidized plain carbon steels, containing 0.16 and 0.79 pct C. A combination of fractography and quantitative metallography on sectioned, deformed specimens permitted separation of the effects of hydrogen on the initiation, growth, and link-up of voids. In both steels, hydrogen was found to have no significant effect on either the initiation of voids at carbides, or early growth of voids, prior to link-up. In the higher carbon steel the fracture surface dimple size increased after hydrogen exposure with no other evident change in the fracture surface appearance; it is therefore inferred that hydrogen primarily assists void growth during link-up in this steel. In the lower carbon steel the fracture appearance changed and a decrease in void size due to hydrogen was found fractographically; thus, both initiation and growth of voids are apparently enhanced during the link-up phase of fracture in this steel. It is hypothesized that these effects may be due largely to a void pressure mechanism if hydrogen is transported by mobile dislocations.

HYDROGEN embrittlement of steel often involves both a change in fracture mode and a loss in ductility, relative to fracture behavior in the absence of hydrogen.[1] However, there have been several cases reported in which no fracture mode change occurred despite moderately large losses in ductility.[1-4] These latter cases offer the possibility for distinguishing which of the substeps involved in the fracture process are predominantly affected by the introduction of hydrogen. One such case is the ductile fracture of spheroidized plain carbon steel.

Ductile fracture occurs by a sequence of initiation, growth, and link-up of microvoids. Hydrogen effects on all three of these contributing events or substeps have been envisaged.[2] In a preliminary study on the effect of hydrogen in 0.8 pct C eutectoid steel, Garber, *et al*[4] attempted to distinguish which, if any, of these substeps were affected. They observed that the introduction of hydrogen caused a measurable increase in the fracture surface dimple size. Since this *increased* dimple size relative to uncharged material occurred at a *smaller* fracture strain, an accelerating effect of hydrogen on void growth and/or link-up was necessarily inferred. In that work,[4] the effect of hydrogen on void initiation was studied by the method of Argon and Im,[5] in which void initiation is quantified by a critical stress. This stress is calculated from the location, along the axis of a deformed and longitudinally-sectioned round tensile specimen, at which the areal density of voids becomes zero. Calculations for two purities of eutectoid steels showed no significant difference in the void initiation stress between hydrogen-free and hydrogen-containing specimens.[4] However, the void growth and link-up processes were not studied directly; their contribution was inferred by elimination.

The purpose of this paper is to describe additional experiments conducted to study in more detail and in a more direct manner the effect of hydrogen on the substeps of void initiation, growth, and link-up. "Initiation" is defined here to mean the process by which the matrix separates from a particle (usually a carbide) to form an observable microvoid. Initiation may occur (in general) over a wide range of strain, from the yield point to well past necking; additional nuclei may also form during the final link-up process.[5,6] In this paper, "initiation" will refer to events prior to link-up unless otherwise noted. Similarly, microvoid growth can occur over the whole range of post-initiation strain, and may be considerably accelerated during link-up, but "growth" in this paper refers to the pre-link-up event. Finally, "link-up" refers to the (poorly-defined) process which terminates plasticity-controlled growth and causes the microvoids to become connected together in a relatively short interval of strain, for example by localized shear.[6,7] Figure 1 is a schematic showing the behavior expected for both the number of microvoids, and their size, with increasing strain. The rather rapid increase in these quantities at a strain near the fracture strain may not correspond to any new physical process, but (partly for experimental reasons) we find it convenient to call this relatively small range of strain the regime of link-up and final fracture.

In the present work, initiation and growth were studied directly by an experimental technique involving the quantitative metallographic study of longitudinal sections of the neck centers of initially-unnotched round tensile specimens deformed plastically to strains between necking and fracture. The sectioning procedure has been described in detail recently by Van Stone and Cox.[7] Plotting of the metallographic parameters as a fraction of strain (or stress) allows for an accurate analytical description of the processes of void initiation and growth. For example, the density of microvoids is assumed to reflect initiation, while the average size of a

R. GARBER, formerly Graduate Student, Department of Metallurgy and Materials Science, Carnegie-Mellon University, is now with Climax Molybdenum Co., Ann Arbor, MI 48105. I. M. BERNSTEIN and A. W. THOMPSON are Professors, Department of Metallurgy and Materials Science, Carnegie-Mellon University, Pittsburgh, PA 15213.

Manuscript submitted October 24, 1979.

ISSN 0360-2133/81/0211-0225$00.75/0

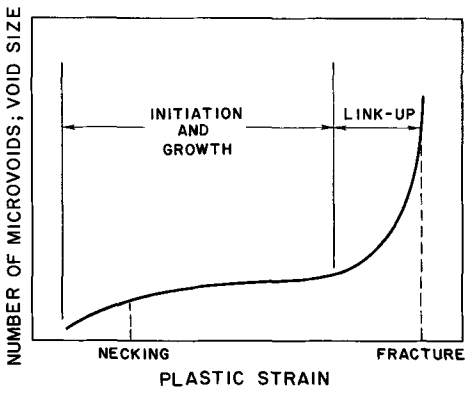

Fig. 1—Schematic illustration of the expected change in number and size of microvoids as a function of strain. The extent of the "link-up" stage is somewhat arbitrary, but can be recognized by a marked steepening of the curve in a plot of this type, usually at a large fraction of the fracture strain.

microvoid is assumed to reflect growth, and hydrogen effects on either should be evident by comparing uncharged with hydrogen-charged specimens. Link-up is difficult to study directly, but inferences regarding it can be drawn by comparing the foregoing metallographic parameters at high strain, with quantitative fractographic observations.

The experimental objectives of the work involved fracture nucleation, so steels of differing carbon content were chosen to permit variation in carbide volume fraction.

EXPERIMENTAL PROCEDURE

Specimen Preparation

The materials used in this study were a laboratory heat of eutectoid carbon steel, the composition of which essentially corresponds to AISI 1080, and a commercial heat of AISI 1018. Compositions of the steels are shown in Table I. The 1080 steel was received in the form of 14.3 mm (9/16 in.) square hot-rolled bar, while the 1018 steel was received in the form of 11.1 mm (7/16 in.) diam cold-drawn rod. The 1080 steel was rough machined to 9.5 mm diam rod prior to heat treatment.

Spheroidized microstructures were produced in both steels by austenitizing, water quenching, and tempering. Austenitizing was conducted in a flowing inert gas atmosphere. The 1080 steel was austenitized at 835 °C for 1 h, quenched in agitated ice water, and promptly tempered at 685 °C for 3 h. The 1018 was austenitized at 1000 °C for 30 min, quenched in agitated 5 pct polyalkylene glycol-water solution,* and tempered at 700 °C for 7 days. Resulting average carbide diameters were 0.9 μm for 1018 and 0.4 μm for 1080.

* Quench severity equivalent to iced brine.[8]

Tension Testing

The tensile specimens were unnotched and had a gage length four times the gage diameter; diameters were 6.35 mm for 1080 steel and 5.1 mm for 1018 steel.

Table I. Composition of Steels (Wt Pct)

Steel	C	Mn	Si	S	P
Eutectoid*	0.79	0.56	0.16	0.019	0.023
AISI 1018	0.16	0.79	0.03	0.016	0.005

* Corresponds to AISI 1080.

Tension tests of both steels were carried out at room temperature using a constant crosshead velocity of 0.02 mm/s (0.05 in./min) for the 1080 steel and 0.002 mm/s (0.005 in./min) for the 1018 steel. Strain was measured with a strain gage extensometer prior to necking, and by micrometer measurements of the neck diameter thereafter.

Hydrogen Charging

Hydrogen was introduced into both steels immediately prior to tensile tests by electrolytic charging under galvanostatic conditions. The shoulders of the specimen were protected by electroplater's stopoff lacquer, and a spiral platinum anode surrounded the specimen which was immersed in a charging solution of 4 pct H_2SO_4, with an addition of 1 mg/l of arsenic to inhibit hydrogen recombination.[9] For the 1080 steel, the current density was 10 mA/cm^2, while for the 1018 steel it was 1 mA/cm^2; for both steels, the charging time was 24 h. These charging conditions were found to produce no irreversible hydrogen damage in either steel.

The hydrogen content produced by electrolytic charging was measured by vacuum hot extraction at 1000 °C, using two or more specimens. For 1080, the hydrogen content was 5 ppm by wt, while for 1018 it was 2 ppm by wt (standard deviation about 20 pct of mean value).

The uniformity of distribution of hydrogen in spheroidized 1080 was evaluated by determining the room temperature effective hydrogen diffusivity using the precision electrochemical permeation method described by McBreen, Nanis and Beck.[10] This value was found to be close to 10^{-6} cm^2/s, an effective diffusivity which is consistent with values recently reported for a spheroidized 1045 steel.[11] Using the standard mathematical solution for transverse diffusion in an infinitely long cylinder,[12] it can be calculated from this effective diffusivity value that the hydrogen concentration in the center of the specimen will be within 2 pct of the surface concentration for the charging time used. While no measurements were made on the 1018 steel, it is well known[13] that the effective diffusivity in spheroidized steel increases with decreasing carbon content, so that the hydrogen distribution in 1018 should have been very uniform.

Following hydrogen charging, specimens of 1018 were electroplated with a thin layer of copper to reduce the loss of hydrogen during transfer to the tensile test machine and subsequent testing at the slower strain rate. Outgassing was sufficiently slower in the 1080 that plating was not required, particularly since a more rapid strain rate was employed.

Fractography and Sectioning

Fracture surfaces of hydrogen charged and uncharged steels were examined in a scanning electron microscope (SEM), with the viewing direction accurately aligned parallel to the tensile axis.

Metallography of the fracture process in both steels was accomplished by the method of sectioning. A series of tensile specimens of each steel (both hydrogen charged, and uncharged) were deformed to strains between necking and fracture. The strained specimens were sectioned longitudinally by carefully surface grinding to within 0.13 mm (0.005 in.) of the midplane, and were then mounted in plastic and metallographically polished to the midplane. All specimens of each steel were carried through the metallographic preparation process as a unit, using automatic equipment (Buehler Automet). Specimens were then lightly etched in saturated picral. The neck centers were examined and the fracture process characterized by quantitative metallography;[14] for most observations, eighty fields of view were measured. The void volume fraction V_V, measured by point counting, was used as an overall measure of the fracture process. The void initiation process was quantified by the areal density of voids, N_A. The void growth behavior was quantified by the average area per void, $\overline{A}$, defined with the void areal fraction A_A as

$$\overline{A} = \frac{A_A}{N_A} = \frac{V_V}{N_A}. \qquad [1]$$

For the 1080 steel, quantitative metallography was carried out on the SEM using a tilt angle of 30 deg and a nominal magnification of 7500 times. The measurements were corrected for tilt foreshortening and for changes in the effective working distance (and thus magnification). For 1018 steel, quantitative metallography was carried out on an optical metallograph at a magnification of 1000 times.

For 1080, assessment of void initiation was also made by the method of Argon and Im.[5] The sectioned, fractured specimens were examined, and N_A was determined as a function of distance from the fracture surface along the tensile axis. To prevent measurement bias, each determination of N_A was made using a photograph taken by a randomizing procedure.

Some of the results of this work were found to contain appreciable scatter, and standard statistical procedures were used as needed. For example, in comparing two sets of data for hydrogen-charged and uncharged specimens, mean values were compared using the standard t test for the difference of two means with variances not necessarily equal.

RESULTS

Tensile Tests

The flow curve for 1080 steel is shown in Fig. 2. Introduction of hydrogen into this steel reduced the true fracture strain from 0.84 to 0.59. This corresponds to a 21 pct loss of reduction of area or RA (from 57 to 45 pct). The loss of RA is smaller than the 60 pct loss obtained in previous work,[4] an observation in keeping with the lower charging current density employed in the present work, which would be expected to lead to a lower hydrogen content. Hydrogen was not found to affect any other portion of the 1080 flow curve within experimental error.

Flow curves for 1018 steel, both uncharged and hydrogen charged, are shown in Fig. 3. In contrast with the 1080, hydrogen caused a small increase of about 5 pct in flow strength. The observed magnitude of the increase is in reasonable agreement with prior observations in 1020 steel by Seabrook, Grant and Carney.[15] Hydrogen also reduced the true fracture strain from 1.61 to 1.04. This corresponds to a 25 pct loss in RA (from 80 to 60 pct).

"Reversibility" of the embrittlement was checked by degassing a charged but unplated specimen of 1018 for 24 h at 160 °C. The RA then obtained was the same as for the uncharged steel. Reversibility was similarly established for the 1080 steel.

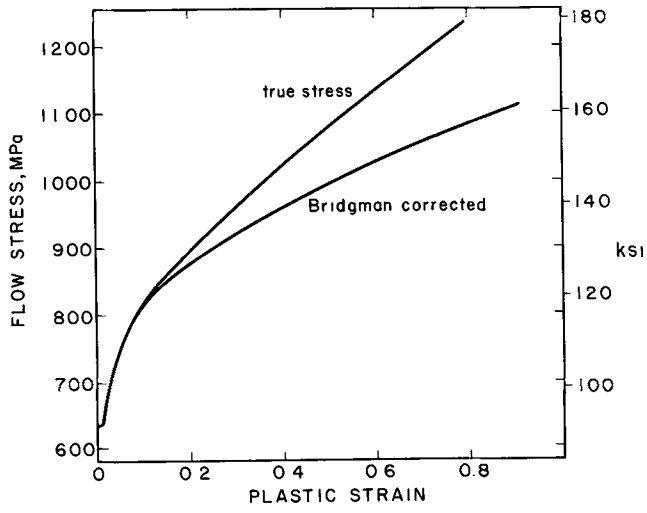

Fig. 2—True stress-true strain relation for 1080 steel. Hydrogen charging did not alter the behavior except for reduced fracture strain.

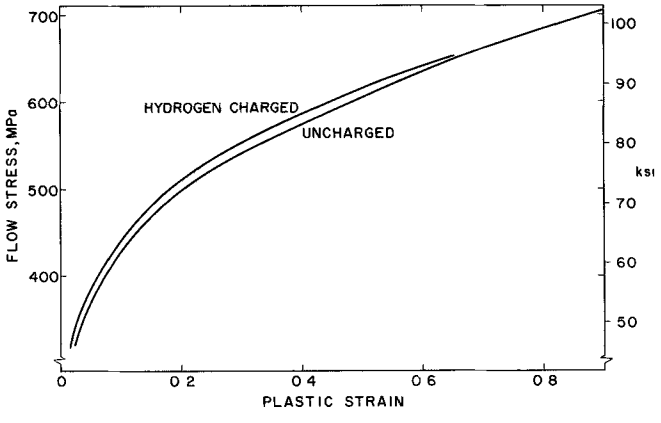

Fig. 3—True stress-true strain relation for 1018 steel. Here hydrogen charging elevated the flow stress by about 5 pct over much of the strain range. Necking strain about 0.25.

Sectioning Studies on 1080 Steel

Void Initiation. Measurements of the number of voids per unit area, N_A, as a function[5] of distance along the tensile axis from the fracture surface, z, are shown in Fig. 4. The data have been fitted by least squares lines of both first order (linear) and second order (quadratic). The z axis intercept of these lines is taken as the point at which voids first initiate.[5] The total interfacial tensile stress at the particle, σ_{rr}, according to Argon and Im,[5] is

$$\sigma_{rr} = Y(\bar{\epsilon}_p) + \sigma_T, \qquad [2]$$

where $Y(\bar{\epsilon}_p)$ is the true flow stress of the matrix at the equivalent plastic strain $\bar{\epsilon}_p$, and σ_T is the hydrostatic stress due to necking of the specimen. The value of σ_{rr} at the point of void initiation is then taken as the particle-matrix interface strength. The equivalent strain

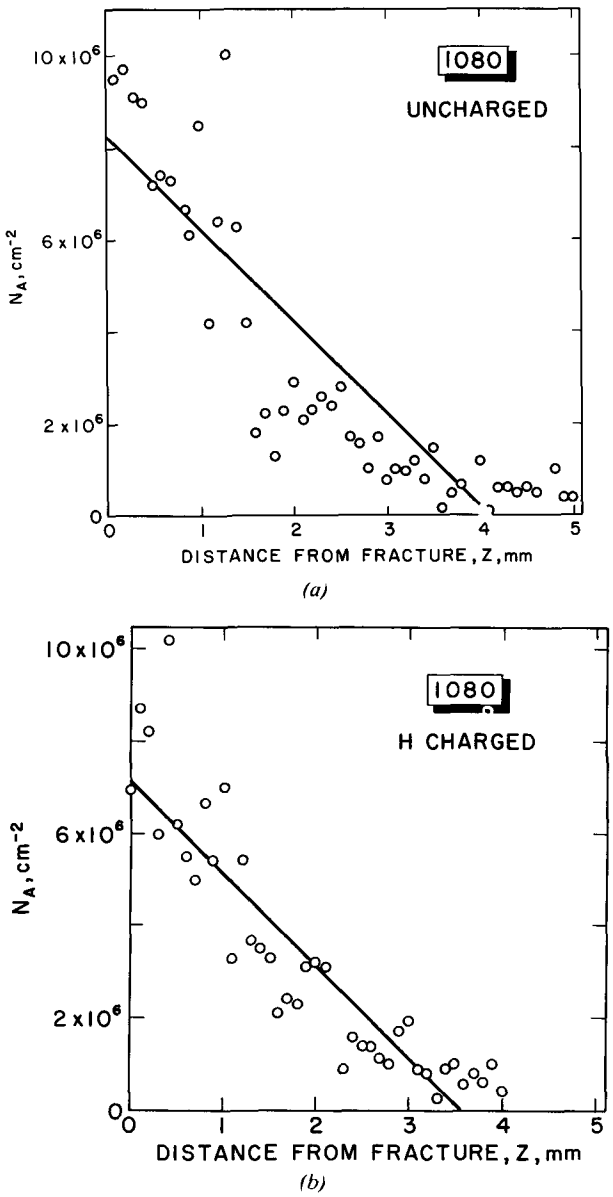

Fig. 4—Number density of microvoids, N_A, as a function of distance along specimen from fracture surface, z, according to procedure described by Argon and Im,[5] for 1080 steel. Least-squares linear fits to data shown by lines. (*a*) Uncharged. (*b*) Hydrogen-charged.

was calculated from the specimen diameter, and the hydrostatic stress was calculated using the extended Bridgman analysis given by Argon, Im, and Needleman.[16]

The void initiation stresses calculated in this way from the linear intercepts were 1020 MPa (148 ksi) for uncharged steel and 1069 MPa (155 ksi) for hydrogen charged steel. Use of the quadratic intercepts lowers these values, but brings the values for the charged and uncharged stresses even closer together, at about 800 MPa. The goodness of fit parameter, defined as the sum of the squares of the deviations between computed and observed points, was smaller for the quadratic than for the linear fits, but the difference was not great, particularly for the hydrogen-charged data, Fig. 4(*b*). Partly for this reason and partly to permit comparison to earlier work,[4] we focus on the values from the linear fits.

As in the earlier work[4] on eutectoid steel, the difference in void initiation stress does not appear to be significant. The standard deviation of Argon and Im's results[5] is 111 MPa, and if the present results are assumed to have the same standard deviation, the difference in the mean values would not be statistically significant. The hydrogen value, 1069 MPa, is somewhat lower than the 1240 MPa observed in the previous work[4] on 1080; this probably results from higher accuracy in the present work, since an SEM with higher void resolution capability was available for the present work.

The Argon and Im method[5] depends on the determination of the point of void initiation by extrapolation. As can be seen in Fig. 4, this lends some uncertainty to the method, since there is a low void density "tail," of about 0.5×10^6 cm^{-2}, on the N_A *vs* z curve. As Cialone and Asaro observed,[17] this tail can be accounted for by measuring the apparent void density remote from the specimen neck and subtracting that value from the distribution. The "base-line" value observed by them[17] was also 0.5×10^6 cm^{-2}. In the present work, such a procedure would raise the void initiation stress by about 15 pct for both charged and uncharged specimens.

Another factor which can affect calculation of the void initiation stress is interaction among particles with locally-higher volume fraction,[18] an effect which should be significant for the overall carbide volume fraction in this steel of about 0.12.* This effect is estimated to raise the present calculated void initiation stresses for both charged and uncharged steel by about 19 pct.[5]. Thus there are several difficulties in obtaining a reliable, absolute value for the carbide interfacial strength. Nevertheless, the point to be noted here is that neither use of different fitting functions, nor varying choices of the "baseline" void density, nor particle interaction, gave rise to a *statistically significant difference* between hydrogen-charged and uncharged specimens.

The Argon and Im method can be regarded as giving only a rather limited basis for comparing void initiation behavior, because it addresses only the earliest stages of

* Argon and Im's measurements[5] on their 1045 steel gave a volume fraction of 0.125; since the phase diagram sets an upper limit of about 0.07 for iron carbides in that composition, the difference presumably comprised MnS and other inclusions.

void initiation; generally the void initiation process continues with increasing strain. A fuller picture of initiation behavior, therefore, can be obtained by a direct comparison of N_A *vs* plastic strain as strain increases.

The measured areal density of voids, N_A, at the neck center of an unfractured specimen, is plotted as a function of plastic strain in Fig. 5. Within the scatter of the data, there is no significant difference between void initiation with or without hydrogen: the difference between each point and the curve shown is probably not significant in view of the ranges of N_A values shown. Thus it may be concluded that in 1080 steel, hydrogen has no effect on either early void nucleation, a process presumably[5] controlled by the ferrite-carbide interface strength, or on observed void densities at strains approaching the fracture strain. This conclusion, that hydrogen does not affect void nucleation in this steel, has been shown by two different methods, Figs. 4 and 5, and the effect of hydrogen on fracture must then be sought in its role in either void growth, link-up, or both.

Void Growth. Void growth in 1080 steel was quantified by measuring the void area fraction, A_A, as a function of strain; this is shown in Fig. 6. This figure shows no evident acceleration of the overall fracture process by hydrogen up to a strain very near the fracture strain for the hydrogen charged steel. Calculation of $\bar{A}$ from Eq. [1] using the data of Figs. 5 and 6 showed that the average area per void, as a function of plastic strain, exhibited no evident effect of hydrogen. However, $\bar{A}$ appears to increase only slightly with strain. This indicates that only the relatively early stages of the fracture process are being observed in the range of strain up to 90 pct of the fracture strain. Pronounced mechanical instability was observed at strains above 90 pct of the fracture strain, and thus data could not be acquired in that range by the sectioning techniques of this study.

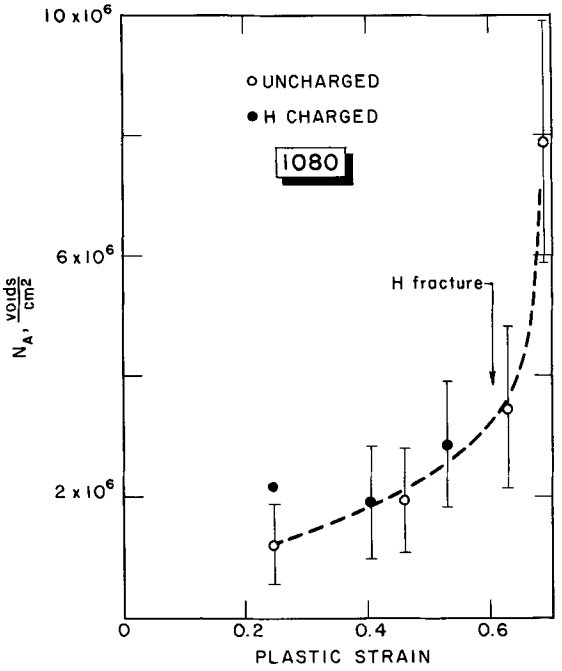

Fig. 5—Microvoid density, N_A, as a function of strain for uncharged and hydrogen-charged 1080 steel. Hydrogen fracture strain indicated by arrow. Data range for separate measurements shown.

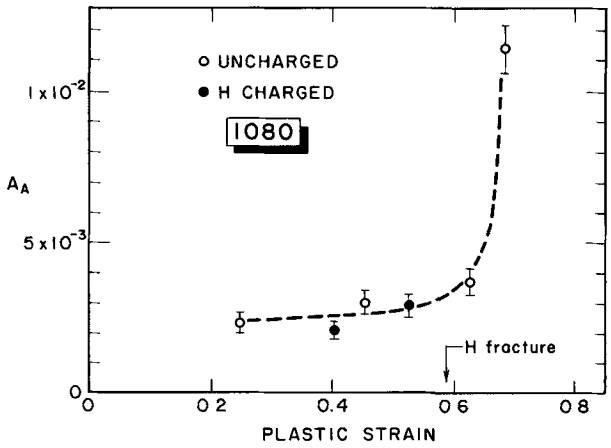

Fig. 6—The area fraction of voids, A_A, as a function of strain for uncharged and hydrogen-charged 1080 steel.

Sectioning Studies of 1018 Steel

Since the commercial 1018 steel used here contained both sulfide stringers and carbides, both of which take part in fracture, these were counted and evaluated separately. The void density N_A, the area fraction A_A, and average area per void $\bar{A}$ for each type of particle is shown in Figs 7 to 9. Points marked "F" in Figs. 7 to 9 were obtained on sectioned, fractured specimens from points near but not at the fracture surface itself. The data obtained are plotted at the fracture strain, but actually correspond to a somewhat smaller strain which was difficult to determine. Moreover, the "F" data may be low due to small voids formed during link-up. Accordingly, these points were ignored in drawing curves through the data.

The carbide-initiated voids will be discussed first. The areal density of voids is unaffected by hydrogen, as was found in the 1080 steel, Fig. 7(*a*). Moreover, although the data are scattered, the void area fraction does not increase with strain more rapidly prior to link-up for hydrogen-charged material than for uncharged, Fig. 8, again in agreemet with the 1080 result. However, in contrast to 1080, the average void area, Fig. 9(*a*), increased earlier and more sharply with strain near fracture for the hydrogen charged steel. While it might be supposed that this increase is due to the onset of void coalescence by impingement of carbide-initiated voids, no noticeable impingement was seen metallographically at strains below the fracture strain.

For sulfide-initiated voids, the areal density increases somewhat more rapidly for hydrogen charged steel, Fig. 7(*b*). Due to the processing of this steel by cold drawing prior to the heat treating of the present work, it is not clear that the observed increase in void density at sulfides may legitimately be regarded as a tensile-test void initiation effect. At least some of these inclusions may be separated from the matrix before tensile testing.[5,6,19] Moreover, the apparent increase in void density with hydrogen might have occurred as a result of

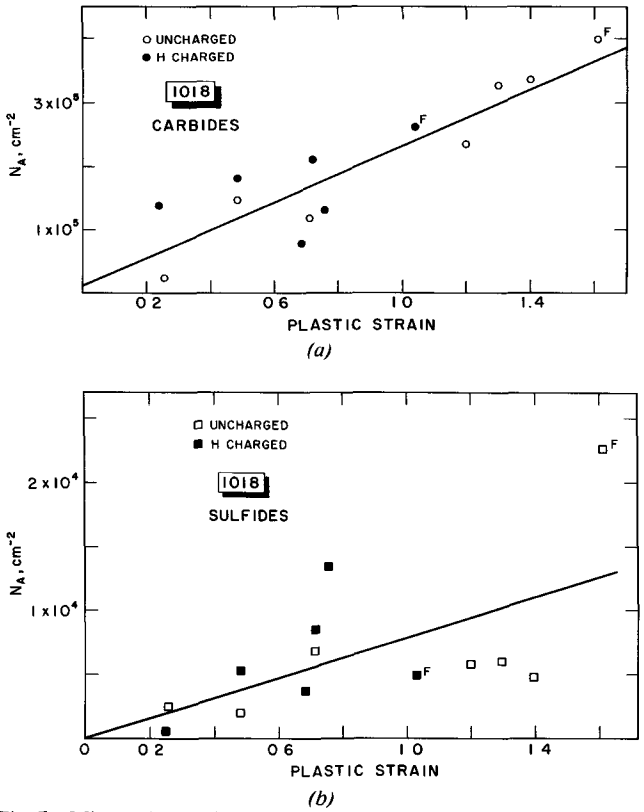

Fig. 7—Microvoid density, N_A, as a function of strain for uncharged and hydrogen-charged 1018 steel. Points marked "F" obtained near the fracture surface of fractured specimens; data are most simply fitted with a straight line. (*a*) Results for voids initiated at carbide particles. (*b*) Results for voids initiated at sulfide stringers and globules.

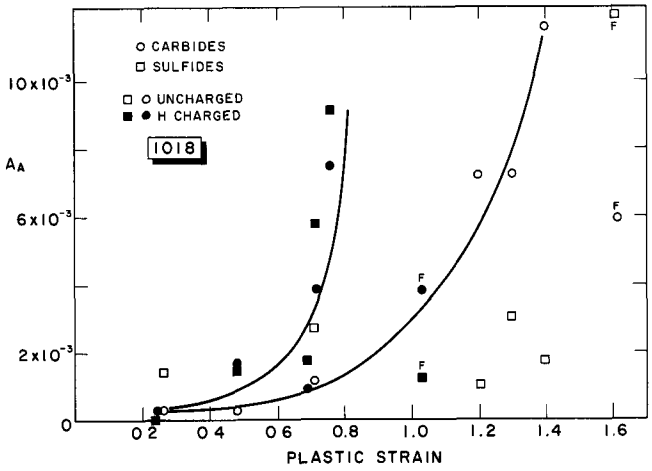

Fig. 8—Area fraction of microvoids, A_A, as a function of strain for hydrogen-charged and uncharged 1018 steel. Carbide-initiated and sulfide-initiated voids were separately measured; lines shown are for carbide data only.

hydrogen charging; hydrogen cracks commonly initiate at sulfide inclusions,[1] so it is reasonable to assume that at least some particle separations were caused during the cathodic charging of this steel. The void area fraction, Fig. 8, and the average area per void, Fig. 9(*b*), also appear to increase more rapidly with strain in the hydrogen-charged steel, although the scatter in Fig. 9(*b*) is considerable. These findings show a slight effect of hydrogen on sulfide-initiated voids which would be consistent with an effect of hydrogen on microvoid growth.

The overall phenomenology of fracture in this 1018 steel may be described as follows: elongated voids start at sulfide inclusion stringers and grow. Meanwhile, smaller equiaxed voids nucleate and grow at carbides. At some point late in the strain history, deformation becomes localized between the large voids and produces the final fracture surface. This description follows the original view by Rogers of the ductile fracture process,[20] with the particular point here being the sulfide nucleation of large voids, while carbides nucleate the smaller voids. Hydrogen's effect is to accelerate slightly the growth of the sulfide-nucleated voids, leading to earlier link-up of the small voids. However, this does not appear to be the primary contribution to reduced fracture strain, since Figs. 7 to 9 show the same pattern as Figs. 5 and 6: a large, almost discontinuous change in the measured parameters which occurs over a relatively small range of strain (link-up) just prior to fracture.

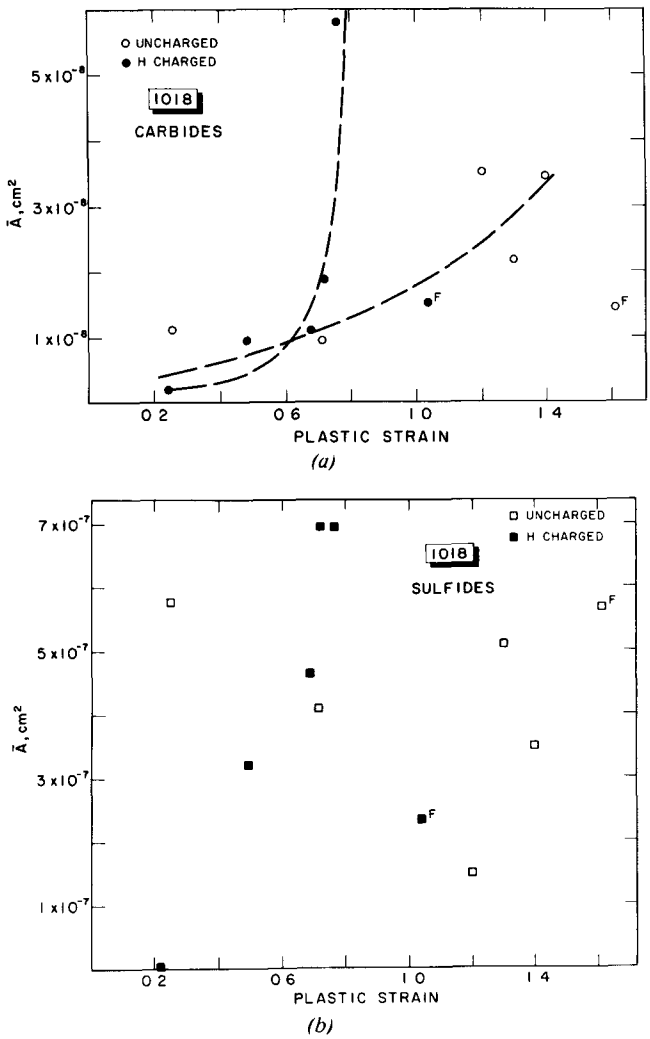

Fig. 9—Average area per void, $\bar{A}$, as a function of strain for uncharged and hydrogen-charged 1018 steel. As in Fig. 8, lines are only shown for carbide results. (*a*) Carbide-initiated voids. (*b*) Sulfide-initiated voids.

A final point should be made regarding the sectioning studies on both the 1018 and 1080 steels. Cialone and Asaro[17] observed ductile void growth and link-up along ferrite grain boundaries in the 1045 steel they studied. Careful examination of all sectioned specimens of both steels in the present study did not reveal a similar effect. Although the carbide volume fraction at boundaries in our steel was somewhat higher than the volume average, as would be expected, no elongated voids or boundary separations of the type reported[17] were observed. We cannot suggest a reason for this difference, unless it lies in different processing histories (the Cialone and Asaro steel[17] was aluminum killed), or even in different metalloid impurity contents, in the respective heats of steel. This is a point which should receive further attention.

Fractography

As a means of assessing the fracture steps which occur very near the fracture strain, *i.e.* link-up, a detailed, quantitative fractographic study of each steel was made.

SEM fractographs of the 1080 steel are shown in Fig. 10. Hydrogen caused an increase in the dimple size of the hydrogen-charged specimen, relative to an uncharged specimen. This increase was quantified by measuring one hundred randomly selected dimples on fracture surfaces of each specimen. Histograms of equivalent-area dimple diameter of the charged and uncharged steel are shown in Fig. 11; the mean dimple size was increased with hydrogen, from 0.89 to 1.15 μm. Given the respective standard deviations, 0.50 and 0.69 μm, the difference in the means is statistically significant at the 99 pct level. A more precise comparison would take into acount the larger dimple size expected at a lower fracture strain,[21] as in the hydrogen case here. Considering only the geometrical effect, it would predict that the hydrogen-charged dimple diameter would be 1.01 μm. The observed 1.15 μm diameter with hydrogen exceeds that value by an amount which is statistically significant at the 99 pct level. Thus even after accounting for differences in fracture strain, hydrogen caused final dimple sizes to be increased in the 1080 steel.

SEM fractographs of the 1018 steel are shown in Fig. 12. In contrast to the 1080, the presence of hydrogen both reduced the ductility and changed the appearance of the fracture in this steel; occasional flat features (about 7 pct areal fraction) were visible on the hydrogen-charged fracture surface in addition to the equiaxed dimples present in the uncharged steel. These fractographic features were studied by precision fractographic matching, which revealed that the ridges found within the flat features match peak to peak. This clearly implies that these features are tear ridges, originating from plastic deformation, and would be classed (in these local areas) as quasicleavage.[22] Similar observations of a hydrogen-induced onset of shallow, flat areas separated by tear ridges, in a material which exhibits dimples without hydrogen, have been made previously.[23]

Measurement of dimple diameters in 1018 gave mean values of 1.91 μm in the uncharged steel, and 1.92 μm when hydogen charged; this difference is not statistically significant. Using the same geometrical prediction[21] referred to previously, the hydrogen-charged dimple diameter is expected to be 2.69 μm; the observed value, 1.92 μm, is less by an amount which is statistically significant at the 99 pct level. Hydrogen, therefore, considerably reduced dimple sizes in 1018 steel on a strain-corrected basis, in direct contrast to 1080 where the reverse was found.

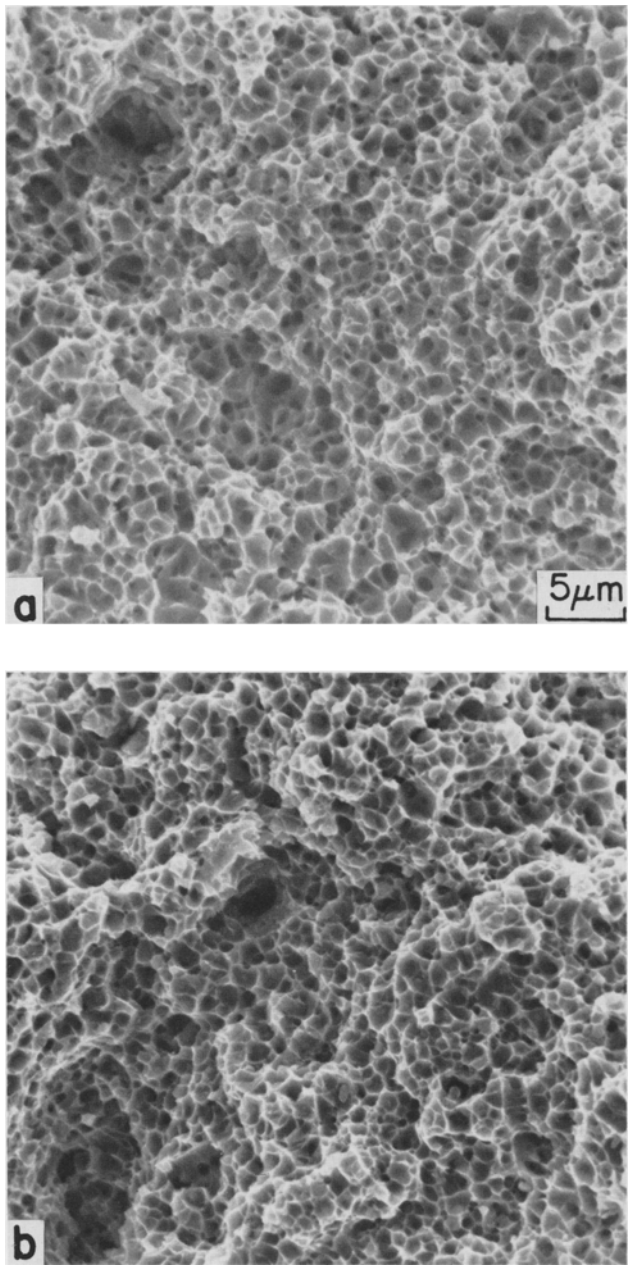

Fig. 10—Typical areas of fracture surfaces in 1080 steel, both at same magnification; viewing direction parallel to tensile axis. (*a*) Uncharged. (*b*)Hydrogen-charged.

DISCUSSION

The details of the experimental observations were discussed as part of the Results section. In this section,

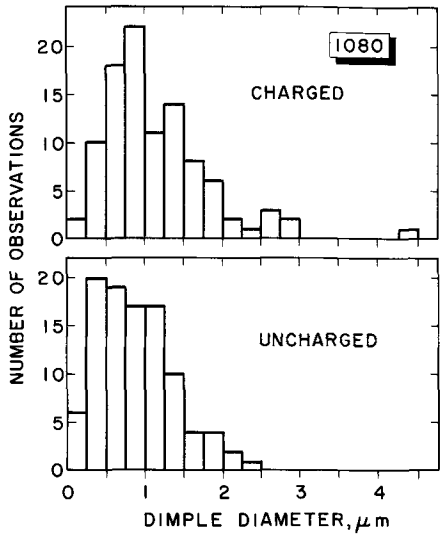

Fig. 11—Histograms of dimple diameters in 1080 steel for uncharged and hydrogen-charged material. Mean dimple size increased with hydrogen, from 0.89 μm to 1.15 μm.

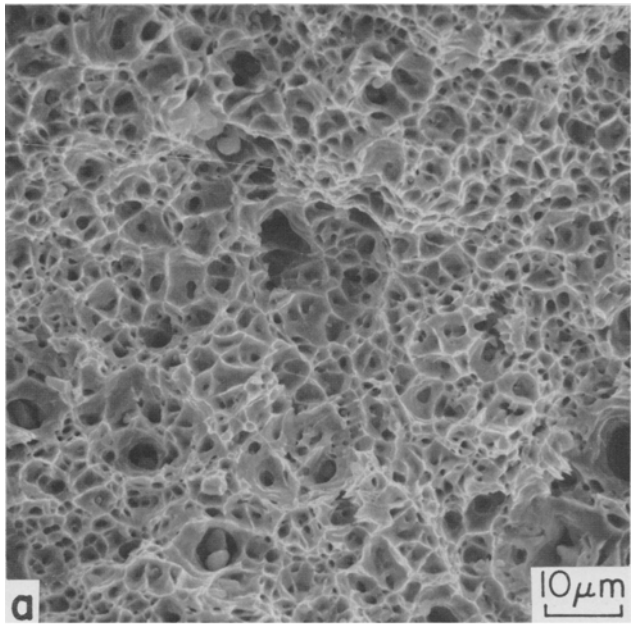

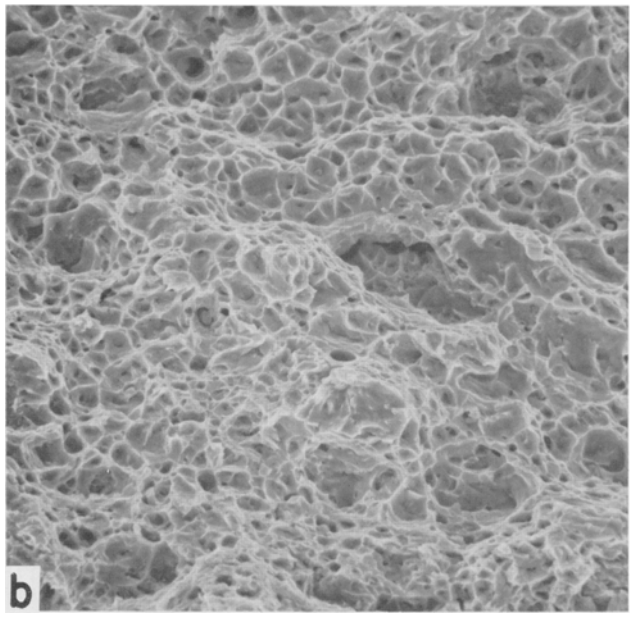

Fig. 12—Fractography of 1018 steel, with viewing direction parallel to tensile axis. (*a*) Uncharged. (*b*) Hydrogen-charged, same magnification as (*a*); discussed in text.

we discuss the overall pattern and implications for our results. First, our data show that void initiation is not assisted or increased by hydrogen: neither initiation of the earliest voids (Fig. 4) in 1080, nor the total void population in both steels (Figs. 5 and 7), are affected over a range of strain up to very near the fracture strain. This is in contrast to what has been inferred for several austenitic materials.[2,21] Second, the void growth process, at least over a relatively large range of strain prior to the onset of final fracture, is not significantly affected by hydrogen in either steel (Figs. 6 and 8), except possibly for sulfide-nucleated voids in 1018. These two points together indicate that the processes of void initiation and growth, as they occur over a large fraction of the total strain to fracture, are not altered by hydrogen in either steel. Yet the fracture strain is significantly reduced by hydrogen. Thus it is the events occurring rather near in strain to final fracture which control the total fracture strain; these coalescence events are referred to above as "link-up."

Link-up can occur either by a rapid acceleration in void growth, or by an enhanced nucleation of microvoids between the existing voids.[20] Reviews of the literature on this point have not been extensive, but both types of process clearly can occur.[2,6] The first question arising from the present results is this: what causes the void density, N_A, and the void size parameters, A_A and $\bar{A}$, to begin to increase very rapidly (Figs. 5, 6, 8 and 9), *i.e.*, to begin link-up, at a particular strain? That question is important because of the second question: how does hydrogen cause that rapid increase to occur at an earlier strain? The usual answer to the first question is attainment of a sufficiently high component of hydrostatic stress, σ_T, to permit rapid growth;[24-26] this also raises the interfacial stress, σ_{rr}, and enhances continued nucleation.[5,18] Thus it is natural to consider two types of hydrogen-assisted mechanisms as answers to the second question: one involves a pressure effect due to hydrogen in voids,[2] while the other involves hydrogen reducing either the strength or the resistance to strain localization of the matrix between voids.[4] Moreover, there is the possibility that both can occur in concert.

The first mechanism mentioned has its origin in Tetelman's refinement[27] of the Zappfe and Sims suggestion[28] that hydrogen precipitation in voids causes a pre-existing internal pressure which aids the external stress in plastic void growth. In this mechanism, the hydrogen transport occurs by lattice diffusion in reponse to the loss of hydrogen from the lattice into the voids and the concomitant concentration gradient. In the present work, hydrogen would probably be regarded as having been transported to voids during the tensile test, since the microvoids are not pre-existing but are initiated during the test.

The likeliness of such a process can be assessed by a mass balance argument, from which the required gas pressure in the voids to cause the observed loss in fracture strain can be reasonably determined. This pressure may be found by extrapolation of the curve for fracture strain as a function of external hydrostatic pressure. Bridgman[29] has shown that the curve is approximately linear. For spheroidized eutectoid (1080) steel, Davidson and Ansell[30] have determined the quantitative pressure dependence; the required internal pressure is 1140 atm. The void volume fraction near fracture for the hydrogen charged steel is 2×10^{-3}. Based on the mean hydrogen content, and the ideal gas law, the calculated pressure* caused by placing all the hydrogen in the neck region into the void volume is 3.9 atm; the ratio of these two pressures is 292. Thus, in order to achieve the required pressure, hydrogen would have to be drawn into the observed neck center volume (due to hydrostatic tension) from a volume equal to or larger than the neck by this ratio.

* Hydrogen at room temperatures, and pressures of the order of 1000 atm, is a rather nonideal gas, so this calculation is conservative, *i.e.*, errs on the low side.

The characteristic linear dimension of the observed neck area is 1.73×10^{-2} cm, so that the transport distance, l, must be larger than this by the cube root of 292, or 6.6. The time for this transport to occur by diffusion would be $t \cong l^2/16D$. In plastically deformed iron, the effective lattice diffusivity is expected to be at least as low as 10^{-6} cm^2/s, so that $t \cong 820$ s. This exceeds the available time (testing time) for fracture by at least a factor of three.

This mechanistic interpretation, that hydrogen diffuses through the lattice into microvoids, is thus only marginally realistic and could be regarded as inadequate. However, mechanisms involving more rapid hydrogen movement, such as dislocation transport, cannot be ruled out. For dislocation transport to be considered a viable alternative, hydrogen would have to be transported at an equivalent effective diffusivity of about 10^{-5} cm^2/s, a value well within the values calculated for iron by any of the available models.[31-33] The present calculation is of particular interest because it shows the feasibility of exerting a pressure of 1140 atm in the relatively large void volume near the fracture strain, not merely the attainment of large pressures at the time of initiation and early growth.[31] Moreover, a conclusion that dislocation transport contributes to ductile fracture in 1080 appears consistent with the findings of Lee, Goldenberg and Hirth,[34] that enhanced cracking in spheroidized 1095 steel was not affected by pre-strain without hydrogen, but was only a function of strain after hydrogen charging.

The foregoing essentially states that an internal hydrogen pressure P (H) can contribute the additional hydrostatic stress needed for the onset of very rapid void growth, *i.e.*, the shallower neck of the hydrogen-charged specimen has a smaller σ_T value, but σ_T (H) + P (H) might equal σ_T for uncharged specimens, at the strain for the onset of link-up. If this does occur, the fracture surface voids should be larger (on a strain-corrected basis[21]) with hydrogen than without. This was observed in the 1080 steel but not in the 1018 steel. Achievement of still higher σ_T values with notched specimens could also enhance nucleation as σ_{rr} rises, Eq. [2]. This may be an explanation for the hydrogen-enhanced void nucleation reported for spheroidized 1095 steel by Lee, *et al.*[34] If so, it is yet another indication that hydrogen can affect mechanical behavior in a variety of ways, depending on the particular experimental design.[35]

The second type of hydrogen mechanism, that of reduced strength or reduced resistance to strain localization of the ligaments between microvoids, was originally proposed by Beachem[36] and has been discussed in several places.[1,2,4,35,37,38] It is difficult to test, although strong indirect support for it has been reported.[4,34] No direct evidence for such an effect was found in our experiments, but the results do not contradict a mechanism of this type, since reduced ligament strength should enhance microvoid growth rates.

An interesting contrast to the 1080 results is provided by 1018, since enhanced void growth was not observed; instead, void sizes *decreased* with hydrogen on a strain-corrected basis. Since this effect evidently corresponds to a considerable increase in nucleation of microvoids, (the increase is calculated[21] to be a factor of about two), it is appropriate to consider how this might occur. One possibility is the increased σ_T due to the deeper necks in 1018. Another possibility is a hydrogen effect on interfacial strength; but with the effect now restricted to the strain regime of link-up. Hydrogen concentrations at particle interfaces could be significantly increased in this regime with or without dislocation transport of hydrogen to particles, because of the locally larger solubility for hydrogen in the lattice due to the hydrostatic tension in the neck, as well as an additional driving force for higher solubility due to the misfit strain field around a particle which has not yet debonded from the matrix.[39] At the same time, it should be emphasized that these apparent nucleation effects are less prominent than in a number of austenitic materials,[2] and accordingly can be interpreted as combined enhancement of nucleation *and* growth.[21] As such, they would support a similar suggestion for 1045 steel.[17,21] The growth effects, if these are occurring, could presumably be rationalized similarly to the 1080 results, above, keeping in mind that nucleation effects must still dominate in order to account for the dimple size decrease.

An additional point on the 1018 is the existence of a partial fracture mode change with hydrogen, Fig. 12(*b*), occupying about 7 pct of the fracture area. These flat, quasicleavage-like features can also be interpreted as supporting pressure-assisted void growth during link-up. McClintock[40] has pointed out that a gas pressure in voids should promote unstable shear of the ligament between voids at a lower void volume fraction than in the absence of the gas. The failure to observe such an effect in 1080 steel may be due to resolution difficulties. In the 1080, a much smaller amount of void growth is required for link-up of voids than in 1018, if it is assumed that all carbides initiate voids which then grow to impingement. It can be calculated[18] that initiation at all carbides would give a ratio of void diameter to particle size of 3.85 for 1018 but only 1.29 for 1080. Thus observation of this kind of link-up effect in 1080

would require higher resolution fractography of dimple edges than was done in this study. The same comment should apply to results on 1095 steel.[34]

It is tempting to consider more detailed models for these growth (or initiation plus growth) effects during link-up. However, an important difficulty exists which makes the value of additional detail uncertain. This difficulty is that the void-initiating particles are distributed randomly, while most theoretical models of fracture contain a fixed spacing. Experimentally, Passoja and Hill[41] found that the number of inclusions per unit area in weldments had a Poisson distribution. In the present study on 1018 steel, the distribution of carbides was also found to be Poisson, as was the distribution of carbide-initiated voids. This randomness of void distribution makes the comparison of models for void link-up problematical (although this randomness has been taken into account by Argon, Im and Safoglu[18] in their study of void *initiation*); it also confounds the calculation of the point at which instability leading to final fracture occurs. Preliminary efforts[42] to model link-up of Poisson-distributed voids are thus of great interest, although they have not yet been tested experimentally even for ductile fracture *without* hydrogen. Until this problem is solved it appears premature to attempt detailed modeling of the effect of hydrogen on the link-up portion of the ductile fracture process.

CONCLUSIONS

The effects of hydrogen on ductile fracture in two spheroidized carbon steels, 1018 and 1080, have been examined. A combination of sectioning and fractography led to the following conclusions:

1) Hydrogen does not assist void initiation at carbides, over a wide range of strain prior to final fracture.

2) Hydrogen does not assist the growth of voids, over most of the wide range of strain prior to final fracture.

3) The final fracture process, called "link-up" in this work, comprises nearly all the effects of hydrogen in reducing fracture strain.

4) In 1080 steel, final dimple size is significantly increased by hydrogen; transport calculations indicate that sufficient hydrogen could be available in microvoids to exert the required pressure to assist growth during link-up, provided the hydrogen is transported via mobile dislocations.

5) In 1018 steel, initiation of microvoids during link-up occurred, together with enhanced microvoid growth. The observation of flat, quasicleavage-like facets in this steel appears consistent with the apparent growth effect inferred for this steel.

ACKNOWLEDGMENTS

We have been greatly helped in this work by extensive discussions with G. M. Pressouyre, J. R. Low and A. S. Argon. The work was supported by the U.S. Office of Naval Research, Grant N00014-75-C-0265.

REFERENCES

1. I. M. Bernstein and A. W. Thompson: *Int. Metall. Rev.*, 1976, vol. 21, pp. 269–87.
2. A. W. Thompson: *Effect of Hydrogen on Behavior of Materials*, A. W. Thompson and I. M. Bernstein, eds., pp. 467–77, TMS-AIME, New York, 1976.
3. I. M. Bernstein, R. Garber, and G. M. Pressouyre: *ibid*, pp. 37–57.
4. R. Garber, I. M. Bernstein, and A. W. Thompson: *Scr. Metall.*, 1976, vol. 10, pp. 341–45.
5. A. S. Argon and J. Im: *Met. Trans. A*, 1975, vol. 6A, pp.839–51.
6. H. C. Rogers: *Ductility*, pp. 31–61, ASM, Metals Park, OH, 1968.
7. R. H. Van Stone and T. B. Cox: *Fractography-Microscopic Cracking Processes,* ASTM STP 600, pp. 5–28, American Society for Testing and Materials, 1976.
8. R. H. Lauderdale: *Met. Prog.*, 1967, vol. 88, December, pp. 79–81.
9. K. Farrell: *Corrosion*, 1970, vol. 26, pp. 105–110.
10. J. McBreen, L. Nanis, and W. Beck: *J. Electrochem. Soc.*, 1966, vol. 113, p. 1218–22.
11. W. M. Robertson and A. W. Thompson: *Met. Trans. A*, 1980, vol. 11A, pp. 553–57.
12. J. Crank: *The Mathematics of Diffusion*, 2nd ed., p. 74, Clarendon Press, Oxford, 1975.
13. Y. Sakamoto and T. Mantani: *Trans. Jpn. Inst. Met.*, 1976, vol. 17, pp. 743–48.
14. J. E. Hilliard: *Trans. TMS-AIME*, 1962, vol. 224, pp. 1201–11.
15. J. B. Seabrook, N. J. Grant, and D. Carney: *Trans. AIME*, 1950, vol. 188, pp. 1317–21.
16. A. S. Argon, J. Im, and A. Needleman: *Met. Trans. A*, 1975, vol. 6A, pp. 915–24.
17. H. Cialone and R. H. Asaro: *Met. Trans. A*, 1979, vol. 10A, pp. 367–75.
18. A. S. Argon, J. Im, and R. Safoglu: *Met. Trans. A*, 1975, vol. 6A, pp. 825–38.
19. T. Gladman, B. Holmes, and I. M. McIvor: *Effect of Second-Phase Particles on the Mechanical Properties of Steel*, pp. 68–78, Iron and Steel Institute, London, 1971.
20. H. C. Rogers: *Trans. TMS-AIME*, 1960, vol. 218, pp. 498–506.
21. A. W. Thompson: *Met. Trans. A*, 1979, vol. 10A, pp. 727–31.
22 C. D. Beachem: *J. Basic Eng. (Trans. ASME, Series D)*, 1965, vol. 87, pp. 299–306.
23. A. W. Thompson and I. M. Bernstein: *Fracture 1977, Proc. 4th Int. Conf. on Fracture*, vol. 2, pp. 249–54, University of Waterloo Press, Waterloo, Ont., 1977.
24. F. A. McClintock: *J. Appl. Mech. (Trans. ASME, Series E)*, 1968, vol. 35, pp. 363–71.
25. J. R. Rice and D. M. Tracey: *J. Mech. Phys. Solids*, 1969, vol. 17, pp. 201–17.
26. D. M. Tracey: *Eng. Fract. Mech.*, 1971, vol. 3, pp. 301–15.
27. A. S. Tetelman: *Fracture of Solids*, D. C. Drucker and J. J. Gilman, eds., pp. 671–708, Gordon and Breach, New York, 1963.
28. C. Zappfe and C. Sims: *Trans. AIME*, 1941, vol. 145, pp. 225–59.
29. P. W. Bridgman: *Studies in Large Plastic Flow and Fracture*, McGraw-Hill, New York, 1952.
30. T. E. Davidson and G. S. Ansell: *Trans. ASM*, 1968, vol. 61, pp. 242–54.
31. J. K. Tien, A. W. Thompson, I. M. Bernstein, and R. J. Richards: *Met. Trans. A*, 1976, vol. 7A, pp. 821–29.
32. J. K. Tien: *Effect of Hydrogen on Behavior of Materials*, A. W. Thompson and I. M. Bernstein, eds., pp. 309–25, TMS-AIME, New York, 1976.
33. H. H. Johnson and J. P. Hirth: *Met. Trans. A*, 1976, vol. 7A, pp. 1543–48.
34. T. D. Lee, T. Goldenberg, and J. P. Hirth: *Met. Trans. A*, 1979, vol. 10A, pp. 199–208.
35. I. M. Bernstein and A. W. Thompson: *Mechanisms of Environment-Sensitive Cracking of Materials*, pp. 412–26, Metals Society, London, 1978.
36. C. D. Beachem: *Met. Trans.*, 1972, vol. 3, pp. 437–51.
37. A. W. Thompson: *Environment-Sensitive Fracture of Engineering Materials*, Z. A. Foroulis, ed., pp. 379–410, TMS-AIME, Warrendale, PA, 1979.
38. A. W. Thompson and I. M. Bernstein: *Advances in Corrosion Science and Technology*, R. W. Staehle, ed., vol. 7, pp. 53–175, Plenum, New York, 1980.
39. H. Y. Yu and J. C. M. Li: *Computer Simulation for Materials Applications*, R. J. Arsenault *et al*, eds., pp. 872–81, TMS-AIME, New York, 1976.
40. F. A. McClintock: *Stress Corrosion Cracking and Hydrogen Embrittlement of Iron Base Alloys*, R. W. Staehle *et al*, eds., pp. 455–72, NACE, Houston, TX, 1977.
41. D. E. Passoja and D. C. Hill: *Fractography-Microscopic Cracking Processes,* ASTM STP 600, pp. 30–46, American Society for Testing and Materials, Philadelphia, 1976.
42. A. Melander: *Mater. Sci. Eng.*, 1979, vol. 39, pp. 57–63.